An Improved 'Gas of Circles' Higher-Order Active Contour Model and Its Application to Tree Crown Extraction*

Péter Horváth[1,2], Ian H. Jermyn[2], Zoltan Kato[1], and Josiane Zerubia[2]

[1] University of Szeged, Institute of Informatics, P.O. Box 652,
H-6701 Szeged, Hungary
Fax:+36 62 546 397
{hp, kato}@inf.u-szeged.hu
[2] Ariana (joint research group CNRS/INRIA/UNSA), Inria,
B.P. 93, 06902 Sophia Antipolis, France
Fax:+33 4 92 38 76 43
{Ian.Jermyn, Josiane.Zerubia}@sophia.inria.fr

Abstract. A central task in image processing is to find the region in the image corresponding to an entity. In a number of problems, the region takes the form of a collection of circles, *e.g.* tree crowns in remote sensing imagery; cells in biological and medical imagery. In [1], a model of such regions, the 'gas of circles' model, was developed based on higher-order active contours, a recently developed framework for the inclusion of prior knowledge in active contour energies. However, the model suffers from a defect. In [1], the model parameters were adjusted so that the circles were local energy minima. Gradient descent can become stuck in these minima, producing phantom circles even with no supporting data. We solve this problem by calculating, via a Taylor expansion of the energy, parameter values that make circles into energy inflection points rather than minima. As a bonus, the constraint halves the number of model parameters, and severely constrains one of the two that remain, a major advantage for an energy-based model. We use the model for tree crown extraction from aerial images. Experiments show that despite the lack of parametric freedom, the new model performs better than the old, and much better than a classical active contour.

1 Introduction

A central problem in image understanding is to find the region R in the image domain corresponding to a particular entity. The crucial quantity is $P(R|I,K)$, the probability that region R corresponds to the entity given the image data I and any prior knowledge K we may choose to include. Typically, to solve such problems automatically, a significant amount of prior knowledge specific to the entity must be included, in particular about region geometry. Generic assumptions, *e.g.* about boundary smoothness, do not suffice.

* This work was partially supported by EU project IMAVIS (FP5 IHP-MCHT99), EU project MUSCLE (FP6-507752), Egide PAI Balaton, OTKA T-046805, and a HAS Janos Bolyai Research Fellowship. We thank the French National Forest Inventory (IFN) for the data.

P. Kalra and S. Peleg (Eds.): ICVGIP 2006, LNCS 4338, pp. 152–161, 2006.

The tree crown extraction problem provides an example. Submetre resolution remote sensing images in principle permit the automatic extraction of the region R corresponding to tree crowns, and the subsequent evaluation of various parameters of importance in forestry and conservation. Particularly in plantations, R takes the form of a collection of approximately circular connected components of similar size. We thus have a great deal of prior knowledge about R, without which trees that are close together or that do not differ much in intensity from the background cannot be extracted correctly. The question is then how to incorporate such prior knowledge into a model for R?

We focus on 'active contour' models [2]. In this context, a region R is represented by its boundary ∂R. $P(R|I,K)$ is constructed implicitly, via an energy functional $E(\partial R) = E_{\mathrm{g}}(\partial R) + E_{\mathrm{i}}(\partial R, I)$, where E_{g} and E_{i} correspond to prior and likelihood. In classical active contours, prior energies E_{g} are constructed from single integrals over the contour. E_{g} includes only local, differential interactions between boundary points, and thus only very simple prior knowledge, *e.g.* boundary smoothness.

To include more complex prior knowledge, longer-range interactions are needed. There is a large body of work that does this implicitly, via a template region or regions to which R is compared, *e.g.* [3,4,5,6]. However, such energies effectively limit R to a bounded subset of region space close to the template(s), which excludes, *inter alia*, cases like tree crown extraction in which R has an unknown number of connected components. 'Higher-order active contours' (HOACs) [7] provide a complementary approach. HOACs generalize classical active contours to include multiple integrals over ∂R. Thus HOAC energies explicitly model long-range interactions between boundary points without using a template. This allows the inclusion of complex prior knowledge while permitting the region to have an arbitrary number of connected components, which furthermore may interact amongst themselves. The approach is very general: classical energies are linear functionals on the space of regions; HOACs include all polynomial functionals.

In [1], a HOAC energy E_{g} was used for tree crown extraction. In this 'gas of circles' model, collections of mutually repelling circles of given radius r_0 are local minima of E_{g}. The model has many potential applications in varied domains, but it suffers from a drawback: such local minima can trap the gradient descent algorithm used to minimize the energy, thus producing phantom circles even with no supporting data. The model as such is not at fault: an algorithm capable of finding the global minimum would not produce phantom circles. This suggests two approaches to tackling the difficulty. One is to find a better algorithm. The other is to compromise with the existing algorithm by changing the model to avoid the creation of local minima, while keeping intact the prior knowledge contained in the model. In this paper, we take this second approach. We solve the problem of phantom circles in [1]'s model by calculating, via a Taylor expansion of the energy, parameter values that make the circles into inflection points rather than minima. In addition, we find that this constraint halves the number of model parameters, and severely constrains one of the two that remain, while improving the empirical success of the model.

In section 2 we present the 'gas of circles' model E_{g}. In section 3, we introduce the inflection point constraint and show how it fixes some of the parameters. In section 4, we apply the model to tree crown extraction. We briefly review previous work, describe our likelihood energy E_{i} and the gradient descent algorithm used to minimize $E = E_{\mathrm{i}} + E_{\mathrm{g}}$, and present experimental results. In section 5, we sum up.

2 The 'Gas of Circles' HOAC Model

A region boundary[1], ∂R, is a map $\gamma : S^1 \to \mathbb{R}^2$ modulo orientation-preserving diffeomorphisms of S^1. The HOAC energy $E_{\rm g}$ used by [1] is then given by[2]

$$E_{\rm g}(\partial R) = \lambda L(\partial R) + \alpha A(R) - \frac{\beta}{2} \iint dp\, dp'\, \mathbf{t}(p) \cdot \mathbf{t}(p')\, \Psi(r(p,p')) \;, \qquad (2.1)$$

where p is a coordinate on S^1; L is the boundary length functional; A is the region area functional; $r(p,p') = |\gamma(p) - \gamma(p')|$; $\mathbf{t} = \partial_p \gamma$; and Ψ is an interaction function that determines the geometric content of the model. In [1],

$$\Psi(z) = \begin{cases} \frac{1}{2}\big(2 - \frac{z}{d} + \frac{1}{\pi}\sin\frac{\pi z}{d}\big) & z < 2d \;, \\ 0 & z \geq 2d \;. \end{cases} \qquad (2.2)$$

With this Ψ, the last term in (2.1) creates a repulsion between antiparallel tangent vectors. This has two effects. First, for particular ranges of α, β, and d ($\lambda = 1$ wlog), circular structures, with a radius r_0 dependent on the parameter values, are stable to perturbations of their boundary. Second, such circles repel one another if they approach closer than $2d$. Regions consisting of collections of circles of radius r_0 separated by distances greater than $2d$ are thus local energy minima. In [1], this was called the 'gas of circles' model.

In order to determine parameter values so that a circle of radius r_0 be an energy minimum, [1] conducted a stability analysis. The energy was Taylor expanded around a circle, and the result was expressed in the Fourier basis. This is the natural basis to use because it diagonalizes (2.1): Fourier components do not interact. The parameters were chosen so that, for a circle of radius r_0, the first derivative of the functional (2.1) was zero (energy extremum) and the second derivative of (2.1) was positive definite (energy minimum). The first constraint determines β in terms of α and d, while the second places constraints on the ranges of the latter two parameters. The values of α and d can further be adjusted so that the energy of the circle is positive (to avoid circle creation everywhere), but not too high. In more detail: if γ_r is a circle of radius r, and $\delta\gamma$ is a small variation of the circle with Fourier components a_k, the energy to second order is

$$E_{\rm g}(\gamma_r + \delta\gamma) = E_0(r) + a_0 E_1(r) + \frac{1}{2}\sum_k |a_k|^2 E_2(k,r) \;,$$

where

$$E_0(r) = 2\pi\lambda r + \pi\alpha r^2 - \pi\beta G_{00}(r) \;, \qquad (2.3a)$$

$$E_1(r) = 2\pi\lambda + 2\pi\alpha r - 2\pi\beta G_{10}(r) \;, \qquad (2.3b)$$

$$E_2(k,r) = 2\pi\lambda r k^2 + 2\pi\alpha - 2\pi\beta\Big[2G_{20}(r) + G_{21}(k,r) + 2irkG_{23}(k,r) + k^2 r^2 G_{24}(k,r)\Big] \;. \qquad (2.3c)$$

[1] We describe the case of one simply-connected connected component. The generalization to multiple multiply-connected connected components is trivial.

[2] The same HOAC energy was first used, but with different parameter values, by Rochery *et al.* [7], to model network shapes.

The G_{ij} are also functions of d. Note that $E_1 = \partial_r E_0$ and $E_2(0, r) = \partial_r E_1$.

Equations (2.3) have the following consequences. First, since the large r behaviour of E_0 is dominated by the α term, we must have $\alpha \geq 0$ for the energy to be bounded below. Second, the condition $E_1(r_0) = 0$ determines β in terms of the other parameters:

$$\beta(r_0) = \frac{\lambda + \alpha r_0}{G_{10}(r_0)} \; . \tag{2.4}$$

Third, because $G_{10} > 0$, $\beta > 0$ is necessary for an extremum. Fourth, although $E_2(k, r_0) > 0$ can only be checked numerically, when $k = 0$, it implies

$$\alpha(r_0) > \beta(r_0)(2G_{20}(r_0) + G_{21}(0, r_0)) = \beta(r_0)\tilde{G}(r_0) \; .$$

3 Monotonic Energy Function

The left of figure 2 shows a plot of the energy of a circle versus radius for parameter values selected according to the above criteria. Viewed as a Gibbs energy, this curve has just the form we require: circles of radius r_0 are metastable (*i.e.* local minima), with an energy that is low but nevertheless higher than that of the empty region. In the absence of supporting data, the global minimum will thus be the empty region, the correct behaviour. A gradient descent algorithm, however, cannot escape from these local minima, meaning that circles of radius r_0, once formed during gradient descent, cannot disappear, even if the data does not support their existence. In practice such circles sometimes do form, which is clearly undesirable. The best solution to this problem would be an algorithm capable of finding the global minimum of the energy. A slightly less ambitious approach, which we take here, involves making a compromise with the algorithm, changing the model to avoid the creation of these local minima, while preserving as much of the prior knowledge as possible.

The idea we will pursue is to adjust the parameters so that the minimum of the curve on the left in figure 2 is replaced by a broad, approximately flat area, as shown in the three rightmost plots in figure 2. Such an energy means that in the absence of image data, a circle will shrink and disappear, whereas small amounts of image data will be sufficient to create a minimum in the flat area, thus producing a stable circle. The natural method to achieve such a broad flat region is to create an energy function that has a single inflection point. If necessary the parameters can then be tweaked to ensure that the gradient of energy wrt radius is positive rather than simply non-negative. It is, however, a nontrivial exercise to find parameter values that result in inflection points. We address this problem via further analysis of the energy (2.1).

We still require that a circle of radius r_0 be stable to sinusoidal perturbations with $k > 0$, but now we also require that such a circle be an inflection point with respect to perturbations with $k = 0$, that is, changes of radius. We will see that these demands are sufficient to fix the prior energy E_{g} up to an overall multiplicative constant and a small range of values for d. More precisely, we still require that $E_1(r_0) = 0$ and $E_2(k, r_0) > 0$ for $k > 0$, but we now require that $E_2(0, r_0) = 0$ too. The first condition gives equation (2.4). The second condition, which follows from equation (2.3c), also relates α and β:

$$\alpha(r_0) = \beta(r_0)\tilde{G}(r_0) \; . \tag{3.1}$$

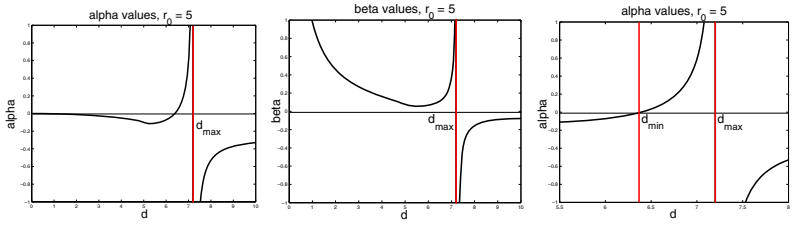

Fig. 1. From left to right ($r_0 = 5.0$ throughout): α plotted against d; β plotted against d; enlarged plot of α near the critical domain

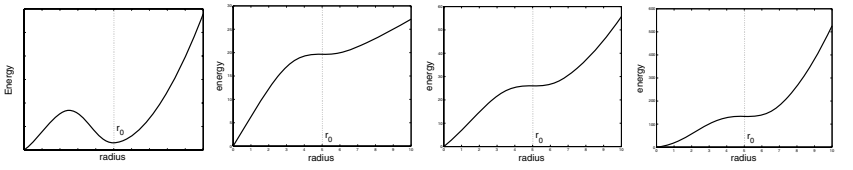

Fig. 2. Plot of E_0 against r for $r_0 = 5.0$. Left: model in [1], with a local energy minimum. Right three: new model, with α and β determined by equations (3.2). Second from left, $d = 6.4$; second from right, $d = 6.8$; far right, $d = 7.2$. For this value of r_0, $d_{\text{min}} = 6.3880$, $d_{\text{max}} = 7.2495$.

We can solve equations (2.4) and (3.1) for α and β, giving

$$\alpha(r_0) = \frac{\lambda \tilde{G}(r_0)}{G_{10}(r_0) - r_0 \tilde{G}(r_0)} \qquad \text{and} \qquad \beta(r_0) = \frac{\lambda}{G_{10}(r_0) - r_0 \tilde{G}(r_0)} \,. \tag{3.2}$$

These equations fix α and β as functions of r_0 and d. Since r_0 is fixed by the application, the only remaining parametric degrees of freedom are the value of d, and the overall strength of the prior term, represented by λ. Recall, however, that we also require α and β to be positive. The question is then how to find values of d for a given r_0 so that $\alpha(r_0) > 0$ and $\beta(r_0) > 0$.

3.1 Determination of d

To illustrate the behaviour we want to understand, figure 1 shows plots of α and β against d for fixed r_0, in this case $r_0 = 5$. There are two critical points, d_{min} and d_{max}. Only for the range $d_{\text{min}} < d < d_{\text{max}}$ are both α and β positive. Our goal is therefore to find d_{min} and d_{max} as functions of r_0.

From equations (3.2), it can be seen that d_{max} arises from a zero in the denominator, while d_{min} arises from a zero in the numerator. It is therefore sufficient to find these zeros in order to find d_{min} and d_{max}. To proceed, we first note a scaling property of G_{00}. The function G_{00} is given by the following integral [1]:

$$G_{00}(r) = \int_{-\pi}^{\pi} dp \, \cos(p) \, r^2 \, \Psi\left(2r \left|\sin\frac{p}{2}\right|\right) \,. \tag{3.3}$$

Since $\Psi(z)$ is a function of z/d only, by pulling d^2 out of the integral we can write G_{00} as $G_{00}(r) = d^2\hat{G}_{00}(r/d)$. Now recall that $G_{10} = \frac{1}{2}\partial_r G_{00}$ and $\tilde{G} = \partial_r G_{10}$. We then find that

$$\tilde{G}(r_0) = \hat{\tilde{G}}(r_0/d) \quad \text{and} \quad G_{10}(r_0) - r_0\tilde{G}(r_0) = d\big(\hat{G}_{10}(r_0/d) - \frac{r_0}{d}\hat{\tilde{G}}(r_0/d)\big)\ , \tag{3.4}$$

where $\hat{G}_{10}(z) = \frac{1}{2}\partial_z\hat{G}_{00}(z)$ and $\hat{\tilde{G}}(z) = \partial_z\hat{G}_{10}(z)$. Thus both numerator and denominator of equations (3.2) can be written, up to multiplication by positive coefficients, as functions of r_0/d. Now, $f(r,d) = \hat{f}(r/d)$ and $f(r,d_0) = 0$ imply $f(ar, ad_0) = 0$ for all $a \in \mathbb{R}$; thus if we determine d_{min} and d_{max} for one value of r_0, we know their values for any r_0.

To determine d_{min} and d_{max} while avoiding iterative numerical procedures to find these points, we use a polynomial approximation to G_{00}:

$$G_{00}(r) = \sum_{n=0}^{\infty} b_n r^n\ .$$

It is easy to show that

$$b_m = \begin{cases} 0 & m < 2\ , \\ \frac{1}{(m-2)!}\int_{-\pi}^{\pi} dp\ \cos(p)\, Y^{(m-2)}(0) & m \geq 2\ , \end{cases} \tag{3.5}$$

where $Y(r) = \Psi(2r|\sin(p/2)|)$. The derivatives of Y evaluated at zero are

$$\frac{Y^{(m)}(0)}{(2|\sin(p/2)|)^m} = \Psi^{(m)}(0) = \begin{cases} 1 & m = 0\ , \\ 0 & m = 1 \text{ or } m \text{ even}\ , \\ (-1)^{\frac{m-1}{2}}\frac{1}{2d}\big(\frac{\pi}{d}\big)^{m-1} & m \geq 3 \text{ and } m \text{ odd}\ . \end{cases}$$

Substituting into equation (3.5) gives b_m:

$$b_m = \begin{cases} 0 & m < 5 \text{ or } m \text{ even}\ , \\ (-1)^{\frac{m-1}{2}}\frac{4(2\pi)^{m-3}}{m!!(m-4)!!}\frac{1}{d^{m-2}} & m \geq 5 \text{ and } m \text{ odd}\ . \end{cases}$$

We can then derive expressions for $\tilde{G}$ and $G_{10} - r\tilde{G}$:

$$\tilde{G}(r) = 2\sum_{\substack{m\geq 3\\ m\ \text{odd}}} \frac{(-1)^{\frac{m+1}{2}}(2\pi)^{m-1}(m+1)}{m!!(m-2)!!}\Big(\frac{r}{d}\Big)^m$$

$$G_{10}(r) - r\tilde{G}(r) = 2d\sum_{\substack{m\geq 4\\ m\ \text{even}}} \frac{(-1)^{\frac{m-2}{2}}(2\pi)^{m-2}}{[(m-3)!!]^2}\Big(\frac{r}{d}\Big)^m\ .$$

We computed the roots of these polynomials including terms up to $m = 49$. The smallest positive roots furnish the values of d_{min} and d_{max}. The result is that $d_{\text{min}} \simeq 1.2776r_0$ and $d_{\text{max}} \simeq 1.4499r_0$. The rightmost three graphs in figure 2 show plots of E_0 against r for $r_0 = 5$, with d values chosen from the domain $d_{\text{min}} < d < d_{\text{max}}$.

4 Tree Crown Extraction

The tree crown extraction problem is important in forestry, and has been much studied. Gougeon [8] uses an automatic valley following method to delineate tree crowns. Larsen [9] uses a template matching method based on a 3D model to find spruce trees. This works well, but requires knowledge of image acquisition and illumination parameters to construct the template. Neither of these methods model the spatial distribution of trees. Perrin *et al.* [10] model a forest as a marked point process with ellipses as marks, thereby including inter-tree interactions. The method in this paper is similar in spirit, although expressed in a very different language. It has the advantage that the tree shape is not hard-constrained, but the disadvantage that it is difficult to apply to dense forest.

4.1 Likelihood Energy and Energy Minimization

We use E_{g}, with parameters fixed as described above, as a prior model for the region R of the image domain corresponding to trees. We also need a likelihood energy $E_{\mathrm{i}}(I, R)$. We will model the image in R, and in the background $\bar{R}$, using Gaussian distributions.[3] We add a term that predicts high gradients along the boundary ∂R:

$$E_{\mathrm{i}}(I,R) = \lambda_i \int dp \mathbf{n}(p)\cdot\partial I(\gamma(p)) + \alpha_i \left[\int_R d^2x \frac{(I(x)-\mu)^2}{2\sigma^2} + \int_{\bar{R}} d^2x \frac{(I(x)-\bar{\mu})^2}{2\bar{\sigma}^2} \right] ,$$

where $\mathbf{n}$ is the (unnormalized) outward facing normal. Note that to facilitate comparison of parameters in the prior energy, we set $\lambda = 1$ in E_{g} and introduce a weight α_i in E_{i}. The parameters μ, σ, $\bar{\mu}$, and $\bar{\sigma}$ are learned from examples using maximum likelihood, and then fixed.

The energy $E = E_{\mathrm{g}} + E_{\mathrm{i}}$ is minimized using gradient descent. The descent equation is

$$\hat{\mathbf{n}} \cdot \partial_t \gamma(p) = -\lambda_i \partial^2 I(\gamma(p)) + \alpha_i \left[\frac{(I(\gamma(p))-\bar{\mu})^2}{2\bar{\sigma}^2} - \frac{(I(\gamma(p))-\mu)^2}{2\sigma^2} \right] - \kappa(p) - \alpha + \beta \int dp' \, \hat{\mathbf{r}}(p,p') \cdot \mathbf{n}(p') \, \Psi^{(1)}(r(p,p')) ,$$

where κ is the curvature of the contour, $\mathbf{r}(p,p') = \gamma(p) - \gamma(p')$, and $\hat{\mathbf{r}} = \mathbf{r}/r$. In the algorithm, it is convenient to represent the boundary by the zero level set of its signed distance function [11]. We use the extended level set framework described in [7] to cope with the nonlocal forces arising from HOAC energies.

4.2 Experimental Results

We tested the model on colour infrared aerial images of poplar stands located in the 'Saône et Loire' region in France, provided by the French National Forest Inventory

[3] We ignore the normalization constant $Z(R) = \int DI \; e^{-E_{\mathrm{i}}(I,R)}$ since in our case it merely changes λ and α, and we are interested in stability of the posterior in the absence of image-dependent terms.

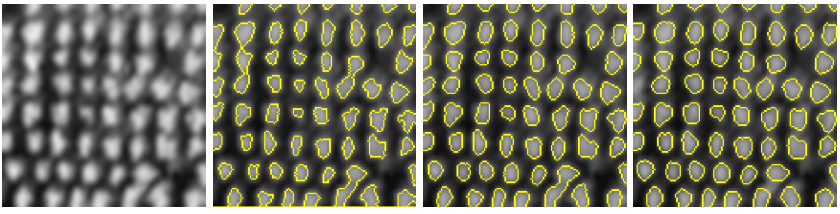

Fig. 3. From left to right: image of poplars ©IFN; the best result with a classical active contour $(70, 0.08, 5.8)$; result with model in [1] $(150, 0.15, 5.8, 4.67, 4.16, 4.16)$; result with new model $(90, 0.08, 5.47, 2.61, 6, 4.16)$.

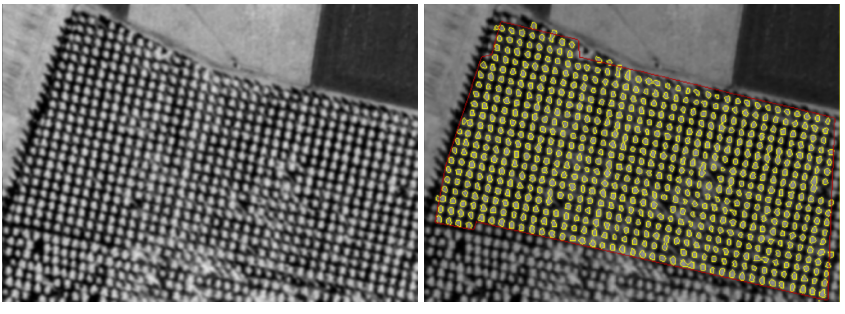

Fig. 4. Left: bigger slice of planted forest ©IFN; right: result using new model $(90, 0.04, 5.49, 2.65, 5, 3.47)$. The contour was initialized to the red line.

(IFN). We compare our new model to a classical active contour ($\beta = 0$), and the model in [1] containing an energy minimum. Note that the new model has three free parameters, λ_i, α_i and d, since the other likelihood parameters are fixed by training, while the other prior parameters are fixed once r_0 is known. The classical active contour also has three free parameters (λ_i, α_i, and α), while the model used in [1] has four (λ_i, α_i, α, and d). The initial contour in all experiments, except that in figure 4, was a rounded rectangle slightly bigger than the image domain. The image values in the region exterior to the image domain were set to $\bar{\mu}$ to ensure that the contour would shrink inwards.

Figure 3 shows four images.[4] On the left is the data. Next comes the best result we could obtain using the same likelihood but setting $\beta = 0$, *i.e.* using a classical active contour. Note how the absence of the quadratic term, which includes the prior shape knowledge, prevents trees from being separated. Next is the result we obtain with the model in [1], while on the right is the result obtained with the new model. Note that the parameter values for the new model, although fixed, nevertheless produce a comparable result. One tree on the border is missing, but on the other hand, two trees are separated that were merged by the old model.

[4] Parameter values in image captions are written in the form $(\lambda_i, \alpha_i, \alpha, \beta, d, r_0)$, truncated if the parameters are not present.

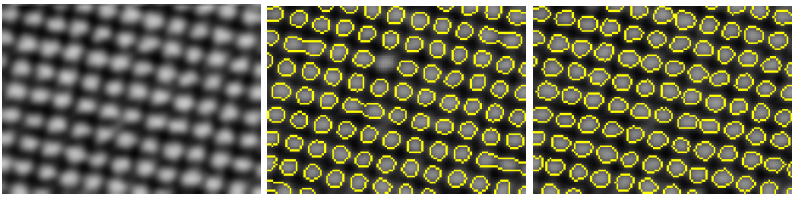

Fig. 5. Left to right: regularly planted poplars ©IFN; result with model in [1] $(40, 0.05, 5, 4.08, 3.47, 3.47)$; result with the new model $(90, 0.07, 5.49, 2.65, 5, 3.47)$.

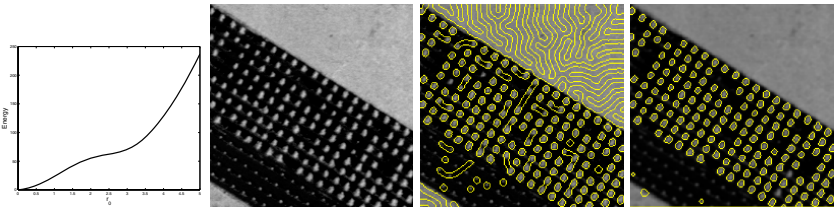

Fig. 6. Left to right: energy of a circle with α slightly greater than the value given by equation (3.2), to create slightly positive gradient everywhere; regularly planted poplars ©IFN; result with model in [1] $(15, 0.008, 4.5, 3.73, 2.51, 2.51)$; result with new model $(40, 0, 6 > 5.40, 2.65, 3.6, 2.51)$.

Figure 4 shows two images. On the left is the data, while on the right is the result obtained using the new model. The initial contour in this experiment was the red line. With a couple of exceptions, the trees are separated and the extraction is accurate.

Figure 5 shows three images. On the left is the data; in the middle is the result obtained with the model in [1]; on the right is the result obtained with the new model. Despite its fixed parameters, the new model produces a better result, finding a tree missed by the old model, and again separating trees that were merged by the old model.

For the experiment in figure 6, we used an α value slightly larger than that given by equations (3.2), in order make E_1 slightly positive for all r. This ensures that in the absence of image data, circles will disappear. The resulting E_0 is shown on the left in the figure. Next comes the data. The aim of the experiment is to detect the older, larger radius trees in the upper part of the plantation area. Third from left is the best result using the model in [1]. Note the phantom regions generated as the contour becomes trapped in local energy minima (the phantom regions in the bright exterior area are also reinforced by the image term). On the right is the result using the new model. With one exception, the phantom regions are eliminated, while the level of error elsewhere is comparable to the old model.

5 Conclusion

The 'gas of circles' model developed by [1] has numerous potential applications in image processing, *e.g.* tree crown extraction from remote sensing images and cell ex-

traction from biological and medical images. The model in [1] suffers, however, from phantom circles created by the fact that circles of a given radius are local energy minima. The requirement that regions consisting of collections of circles of a given radius be inflection points rather than local minima solves this problem. In addition, the requirement halves the number of model parameters, and severely constrains one of the two that remain, a major advantage for an energy-based model. Despite the small remaining freedom to adjust the parameters, experiments on the tree crown detection problem show that the new model performs comparably or better than the old local minimum model, and much better than a classical active contour.

References

1. Horváth, P., Jermyn, I.H., Kato, Z., Zerubia, J.: A higher-order active contour model for tree detection. In: Proc. International Conference on Pattern Recognition (ICPR), Hong Kong, China (2006)
2. Kass, M., Witkin, A., Terzopoulos, D.: Snakes: Active contour models. International Journal of Computer Vision **1** (1988) 321–331
3. Cremers, D., Kohlberger, T., Schnörr, C.: Shape statistics in kernel space for variational image segmentation. Pattern Recognition **36** (2003) 1929–1943
4. Foulonneau, A., Charbonnier, P., Heitz, F.: Geometric shape priors for region-based active contours. Proc. IEEE International Conference on Image Processing (ICIP) **3** (2003) 413–416
5. Paragios, N., Rousson, M.: Shape priors for level set representations. In: Proc. European Conference on Computer Vision (ECCV), Copenhague, Danemark (2002) 78–92
6. Leventon, M., Grimson, W., Faugeras, O.: Statistical shape influence in geodesic active contours. In: Proc. IEEE Computer Vision and Pattern Recognition (CVPR). Volume 1., Hilton Head Island, South Carolina, USA (2000) 316–322
7. Rochery, M., Jermyn, I.H., Zerubia, J.: Higher order active contours and their application to the detection of line networks in satellite imagery. In: Proc. IEEE Workshop Variational, Geometric and Level Set Methods in Computer Vision, at ICCV, Nice, France (2003)
8. Gougeon, F.A.: Automatic individual tree crown delineation using a valley-following algorithm and rule-based system. In Hill, D., Leckie, D., eds.: Proc. Int'l Forum on Automated Interpretation of High Spatial Resolution Digital Imagery for Forestry, Victoria, British Columbia, Canada (1998) 11–23
9. Larsen, M.: Finding an optimal match window for Spruce top detection based on an optical tree model. In Hill, D., Leckie, D., eds.: Proc. of the International Forum on Automated Interpretation of High Spatial Resolution Digital Imagery for Forestry, Victoria, British Columbia, Canada (1998) 55–66
10. Perrin, G., Descombes, X., Zerubia, J.: A marked point process model for tree crown extraction in plantations. In: Proc. IEEE International Conference on Image Processing (ICIP), Genova, Italy (2005)
11. Osher, S., Sethian, J.A.: Fronts propagating with curvature dependent speed: Algorithms based on Hamilton-Jacobi formulations. Journal of Computational Physics **79** (1988) 12–49